Achieving Ultralong Spin Coherent Time of Single Nitrogen Vacancy Centers in Diamond

Xiaoran Zhang(张晓冉)[1,2], Xinyu Zhuang(庄新宇)[1], and Xiaobing Liu(刘晓兵)[1,2*]

[1]*Laboratory of High Pressure Physics and Material Science (HPPMS), School of Physics and Physical Engineering, Qufu Normal University, Qufu 273165, China*

[2]*Advanced Research Institute of Multidisciplinary Sciences, Qufu Normal University, Qufu 273165, China*

(Received 10 March 2025; accepted manuscript online 25 March 2025)

Single negatively charged nitrogen vacancy (NV^-) centers in diamond have emerged as promising platforms for quantum information science, where long coherence times are essential for advancing quantum technologies. However, traditional fabrication methods often introduce lattice damage during the irradiation process used to create vacancies, significantly impairing the spin coherence properties of NV^- centers. In this study, we systematically investigate high-pressure/high-temperature (HPHT) annealing as a non-destructive approach to generate high-coherence single NV^- centers and elucidate the underlying mechanisms. Our results reveal that the distortion of the lattice field significantly influences the preferential formation of NV^- centers at the interface of the ⟨111⟩-growth sector during diamond crystallization. Moreover, HPHT annealing effectively mobilizes nitrogen and vacancies, significantly promoting the formation of single NV^- centers. This process also mitigates the influence of the distortion of the lattice field, resulting in a marked enhancement of coherence properties, with T_2 times reaching 578 μs. Notably, a naturally formed single NV^- center in a low-stress region achieves an exceptional T_2 time of 721 μs, representing one of the highest values reported for diamonds with natural ^{13}C abundance. Building on these insights, we have successfully achieved controlled, large-scale fabrication of high-coherence single NV^- centers, providing essential guidance for future efforts to further enhance their coherence and establishing a robust foundation for their application in quantum technologies.

DOI: 10.1088/0256-307X/42/4/047601 CSTR: 32039.14.0256-307X.42.4.047601

The nitrogen-vacancy (NV) center in diamond is a point defect formed by a substitutional nitrogen atom (P1) adjacent to a carbon vacancy.[1] This spatially dispersed NV^- center, referred to as the single NV^- center, demonstrates exceptional spin coherence times, outstanding optical stability, precise addressability, and high-fidelity quantum control.[2–4] These remarkable characteristics establish single NV^- centers as a leading solid-state quantum systems for applications in quantum computing,[5–7] quantum networks,[8,9] and high-resolution quantum sensing.[10–12] The spin coherence properties are fundamental to the functionality of NV^- centers, as it influences the fidelity of quantum state readout, the duration of quantum entanglement, and the sensitivity of NV-based quantum sensors.[13–16] The spin coherence properties are primarily influenced by dipolar interactions with paramagnetic impurities, such as P1 and ^{13}C,[17] as well as local lattice strain.[15] To optimize quantum performance, high-purity diamond substrates produced via chemical vapor deposition (CVD) are preferred, particularly those with P1 concentrations below 5 ppb.[18] However, the spontaneous formation of NV^- centers during diamond growth occurs only in a limited fraction, which does not suffice to meet the increasing demands of quantum technologies.

Over the years, a variety of fabrication strategies have been developed, utilizing a combination of ion implantation,[19–21] laser or electron irradiation,[22–24] and thermal treatments.[24,25] Although these techniques have effectively facilitated the creation of single NV^- centers, they also cause damage to the diamond lattice through bond disruptions and the introduction of interstitial atoms.[26] This lattice damage subsequently degrades the coherence properties of solid-state qubits,[19,27] even following extensive annealing. Furthermore, the fabrication process often unintentionally introduces an excessive concentration of vacancies, resulting in the unwanted conversion of nitrogen to NV^0.[28] This conversion not only increases background fluorescence but also impairs the spin state readout.[29] Moreover, the optimal annealing temperature for NV^- formation (1100–1200 °C) frequently leads to diamond graphitization.[30] These inherent limitations highlight the pressing need for an implantation-free synthesis strategy that can produce NV^- centers with enhanced spin and optical properties in a more robust and scalable manner.

At elevated pressures (e.g., 5.5 GPa), diamond maintains its thermodynamic stability, allowing high-pressure/high-temperature (HPHT) annealing to effectively suppress graphitization and enable defect engineer-

*Corresponding author. Email: xiaobing.phy@qfnu.edu.cn

© 2025 Chinese Physical Society and IOP Publishing Ltd. All rights, including for text and data mining, AI training, and similar technologies, are reserved.

ing over a wider temperature range.[31,32] Additionally, HPHT diamonds demonstrate superior crystalline quality compared to CVD-grown diamonds, positioning them as an excellent substrate for NV^- center fabrication.[15,33,34] In our previous study, we observed high-coherence NV^- centers in type-IIa diamonds annealed at 1500 ℃ under 5.5 GPa.[31] However, the mechanisms underlying their formation and the enhancement of their coherence properties remain unclear. This lack of clarity hinders the precise and reproducible fabrication of NV^- centers with customized quantum characteristics,[15,33] underscoring the necessity for further investigation. In this study, we systematically investigate the formation mechanisms of single NV^- centers in HPHT diamonds. By employing NV^- centers as nanoscale probes of their local environment, we demonstrate that lattice strain significantly influences their coherence properties. These findings enhance our understanding of NV^- center formation and pave the way for the development of high-fidelity, high-coherence quantum defects in diamond.

High-quality type-IIa single crystals with diameters of 6–7 mm were synthesized via temperature gradient growth (TGG) methods under HPHT conditions in a China-type cubic large volume press (SPD-6 × 1800; see Fig. S1 in the Supporting Information). High-purity graphite (99.99 wt% purity) served as the carbon source, while Fe–Ni alloys acted as the catalyst. To facilitate nitrogen removal, aluminum (1.0 wt%) and titanium (0.5 wt%) were added to the starting materials. For the diamond growth process, synthetic diamond single crystals (∼ 0.4 mm) were utilized as seed crystals under pressures of 5.5–5.8 GPa and temperatures of 1350–1400 ℃. Extended runtimes of up to 60 hours promoted the growth of larger diamonds. The resulting HPHT products were then dissolved in a hot mixed nitric acid solution, comprising H_2SO_4 and HNO_3 in a 2 : 1 weight ratio, to remove residual graphite and metal catalysts. The final high-quality single-crystalline type-IIa diamonds are colorless, as depicted in Fig. 1(a).

Figure 1(b) presents the typical FTIR spectra of the synthesized diamond. The characteristic peaks enclosed within the red-dashed region correspond to the sp^3 C–C bonds in diamond.[35] Notably, the absence of absorption peaks associated with C–N bonds at 1130 and 1344 cm^{-1} confirms that the sample is a type-IIa diamond.[36] Following synthesis, selected diamonds were cut and polished into parallel slices, primarily oriented along the ⟨111⟩ and ⟨100⟩ directions, with a thickness of approximately 1–2 mm, for further characterization. Figure 1(c) displays the photoluminescence (PL) spectra recorded at both the interface and the center of the ⟨111⟩-growth sector. Notably, NV^- centers (with a zero-phonon line at 638 nm) and NV^0 centers (at 575 nm) are predominantly located at the interface, while they are absent in the central region. This observation enhances our understanding of the preferential formation of NV^- centers within the ⟨111⟩-growth sector, adding depth to insights from previous studies.[31] Figure 1(d) presents confocal PL mapping of the ⟨111⟩- and ⟨311⟩-growth sectors, highlighting the distinct edges corresponding to NV^- centers' locations based on diamond growth orientations. The fluorescence intensity diminishes progressively with increasing distance from the interface, suggesting a decrease in NV^- center density. Notably, single NV^- centers emerge at distances greater than 200 μm from the interface [see Fig. 1(d) and Fig. S2 in the Supporting Information], but they become undetectable beyond 700 μm [Fig. 1(f)].

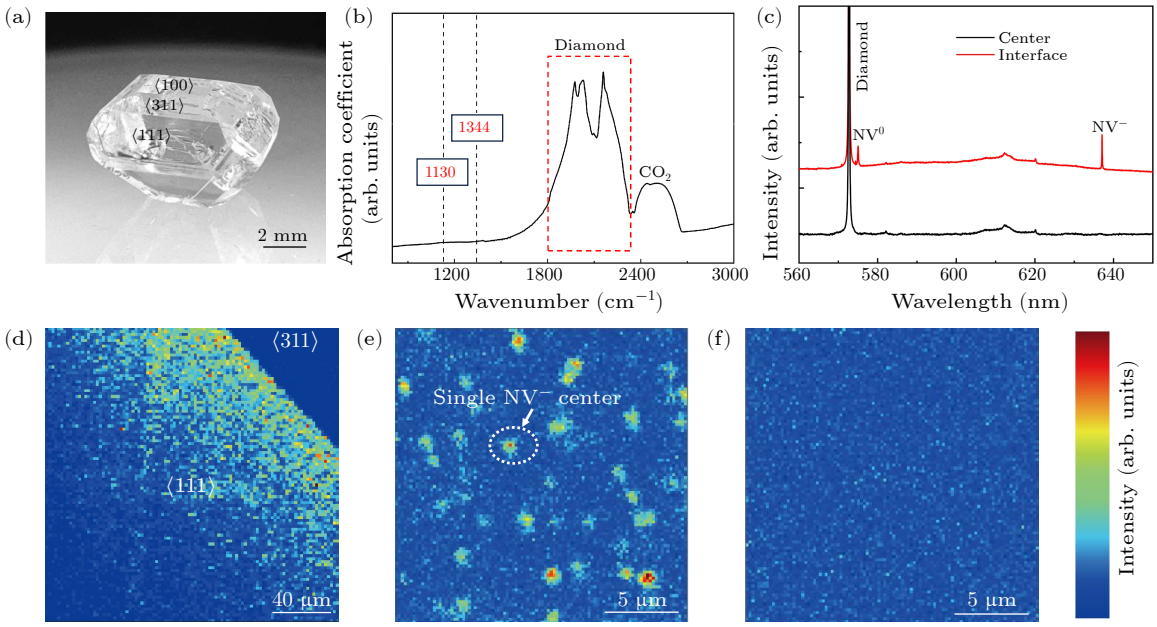

Fig. 1. Formation of single NV^- centers in as-grown diamond. (a) Optical image and (b) FTIR spectra of the synthesized type-IIa diamond. (c) PL spectra obtained from the interface (top) and the center (bottom) of the ⟨111⟩-growth sector, excited with 532 nm lasers at −190 °C. (d) Distribution of NV^- centers. (e) and (f) Confocal images captured at distances of 400 μm (e) and 700 μm (f) from the interface between ⟨311⟩ and ⟨111⟩ growth sectors, revealing single NV^- centers at the interface of ⟨111⟩ growth section.

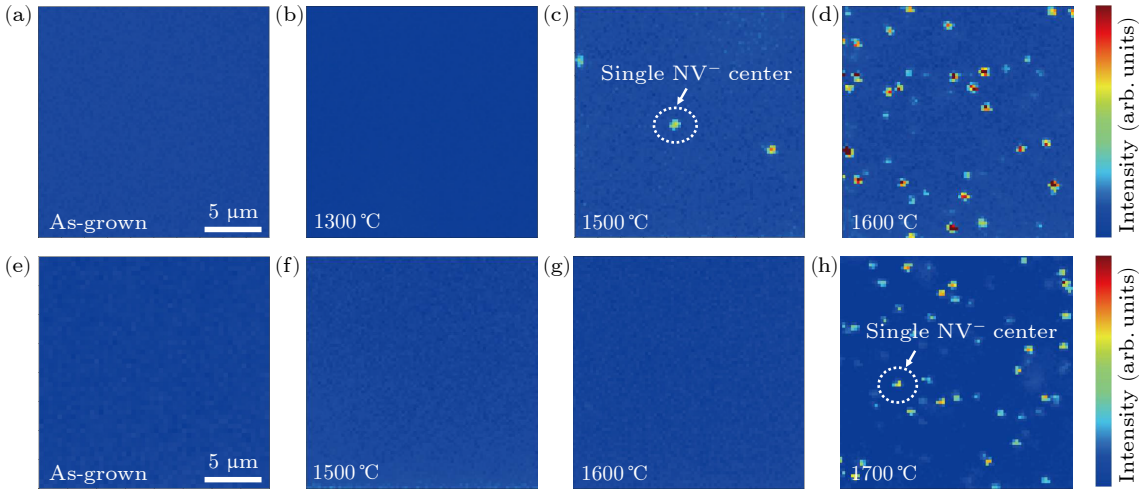

Fig. 2. Generation of single NV^- centers through HPHT annealing treatment. (a) and (b) show confocal images of the ⟨111⟩-growth sector before and after annealing at 1300 ℃, respectively. Subsequent images (c) and (d) depict the effects of treatments at 1500 ℃ and 1600 ℃, revealing that single NV^- centers emerge following annealing at 1500 ℃, with their density further increasing at 1600 ℃. (e) through (h) present 2D confocal images of the ⟨100⟩-growth sector, showcasing the region before (e) and after HPHT treatment at 1500 ℃ (f), 1600 ℃ (g), and 1700 ℃ (h). Notably, single NV^- centers are formed following annealing at 1700 ℃.

We performed annealing treatments of the samples under a pressure of 5.5 GPa and a maximum annealing temperature of 1700 ℃, without observing any graphitization. Figure S3 presents the temperature-dependent PL spectra for the ⟨111⟩-growth sector, revealing that the PL intensity of the NV^- centers remained nearly constant after annealing at 1300 ℃. In contrast, a significant increase in PL intensity was noted following annealing at 1500 ℃. Remarkably, after annealing at 1500 ℃, single NV^- centers appeared in the previously NV-free central region, exhibiting a density of approximately 9 per $(100\,\mu m)^2$, as illustrated in Figs. 2(a)–2(d). Increasing the annealing temperature to 1600 ℃ resulted in a notable rise in density, reaching approximately 140 NV^- centers per $(100\,\mu m)^2$. Figures 2(e)–2(h) display the temperature-dependent confocal PL mapping of the ⟨100⟩-growth sector, revealing that no NV^- centers were formed at temperatures below 1700 ℃. In contrast, annealing at 1700 ℃ led to the detection of spatially dispersed single NV^- centers, with a density of approximately 327 per $(100\,\mu m)^2$. Given the challenges associated with forming NV^- centers in type-IIa diamonds through post-growth techniques at ambient pressure, our findings suggest that HPHT conditions significantly enhance the activation and mobility of nitrogen and vacancies, thereby facilitating NV^- center formation. Furthermore, the results indicate that NV^- centers in the ⟨111⟩-growth sector form at lower temperatures compared to the ⟨100⟩-growth sector, implying a reduced formation energy in the former.

We employed standard free-induction decay (FID) and spin echo measurements to quantify the spin coherence of these single NV^- centers. Figures 3(a) and 3(b) present the measurement signals from a single NV^- centers located 200 μm from the interface. The typical electron spin dephasing time T_2^* for this NV^- centers is measured at 0.6 μs, while the spin coherence time T_2 is approximately 74 μs. Consequently, the coherence properties of the NV^- centers were found to be relatively unremarkable. Figure 3(c) displays the zero-field ODMR spectrum, where Lorentzian fitting indicates a splitting value of 5.37 MHz. This value considerably exceeds that generated solely by the geomagnetic field, indicating the influence of a distortion of the lattice field. Figures 3(d) and 3(e) illustrate the coherence measurements of a single NV^- center located 200 μm from the interface following annealing at 1300 °C. Both T_2 and T_2^* showed marked improvements, with T_2^* increasing to 1.74 μs, over a threefold enhancement and T_2 rising to 317 μs, reflecting more than a fourfold increase. Additionally, NV^- centers situated 400 μm and 600 μm from the interface also exhibited improved coherence times post-annealing at 1300 °C, as detailed in supplementary Figs. S4 and S5.

Subsequent zero-field ODMR measurements indicated a significant reduction in zero-field splitting, which decreased to 3.85 MHz (Fig. 3(f)). Figure 3(g) summarizes the changes in zero-field splitting for single NV^- centers at different distances from the interface following annealing. Remarkably, the zero-field splitting of NV^- centers formed at the interface decreased to approximately 3.8 MHz, a value comparable to that of newly formed NV^- centers created at 1700 ℃. Raman spectroscopy was conducted before and after annealing at both the interface and the center of the ⟨111⟩-growth sector. Notably, both regions exhibited a blue shift of 0.4 to 0.5 cm^{-1} in the diamond Raman peaks following annealing at 1300 ℃. This shift indicates a significant reduction in internal stress and an improvement in the uniformity of stress distribution after the HPHT annealing treatment. Consequently, the reduction in strain significantly extended the T_2 times of the NV^- centers, while the enhanced uniformity in stress distribution further improved T_2^*. Furthermore, we observed that the distortion of the lattice field gradually diminishes with

increasing distance from the interface, correlating with the distribution of NV$^-$ center density. This finding suggests that distortion of the lattice field plays a crucial role in facilitating the preferential growth of NV$^-$ centers.

Figure 4 illustrates the spin coherence properties of NV$^-$ centers generated in HPHT diamond. We performed FID measurements on six single NV$^-$ centers produced after HPHT annealing, one located in the ⟨100⟩-growth sector and the remaining five in the ⟨111⟩-growth sectors. The spin dephasing times T_2^* for these NV$^-$ centers, following HPHT treatment, exceed 1.2 µs, with a maximum value of 2.67 µs observed (see Fig. S6). This result is comparable to the highest values reported for quantum-grade CVD diamonds, as shown in Fig. 4(a). Additionally, spin echo measurements were conducted on nine single NV$^-$ centers, comprising two from the ⟨100⟩-growth sector and seven from the ⟨111⟩-growth sectors. All NV$^-$ centers in the ⟨100⟩ growth region demonstrate values greater than 200 µs (refer to Fig. S7), while those in the ⟨111⟩ growth region achieve even higher values, surpassing 300 µs, with a maximum recorded at 578 µs. This performance is significantly superior to that of NV$^-$ centers produced in CVD diamonds through destructive techniques, such as ion implantation and laser writing [Fig. 4(b)]. Notably, we also identified a naturally formed single NV$^-$ center situated far from the interface in the as-grown type-IIa diamond. Raman spectroscopy and zero-field ODMR measurements indicate that this region exhibits significantly lower growth-induced stress compared to the interface (Fig. S8). Subsequently, we evaluated the spin coherence properties of this center. As illustrated in Fig. 4(c), the spin dephasing time T_2^* reaches 2.59 µs, which is sufficient to resolve the host ^{14}N and nearby ^{13}C nuclear spins, as indicated by the beating feature observed in Fig. 4(c). Spin echo measurements reveal that the spin coherence time, T_2, of this NV$^-$ centre is approximately 721 µs, marking the longest spin coherence time reported for NV$^-$ centers in diamonds with natural ^{13}C abundance. [17]

In this study, we systematically investigated the formation of high-coherence single NV$^-$ centers through HPHT annealing, elucidating the underlying mechanisms. Our findings demonstrate that a distortion of the lattice field promotes the preferential formation of NV$^-$ centers at the interface of the ⟨111⟩-growth sector. Notably, HPHT annealing enabled the widespread formation of dispersed single NV$^-$ centers in previously unoccupied regions,

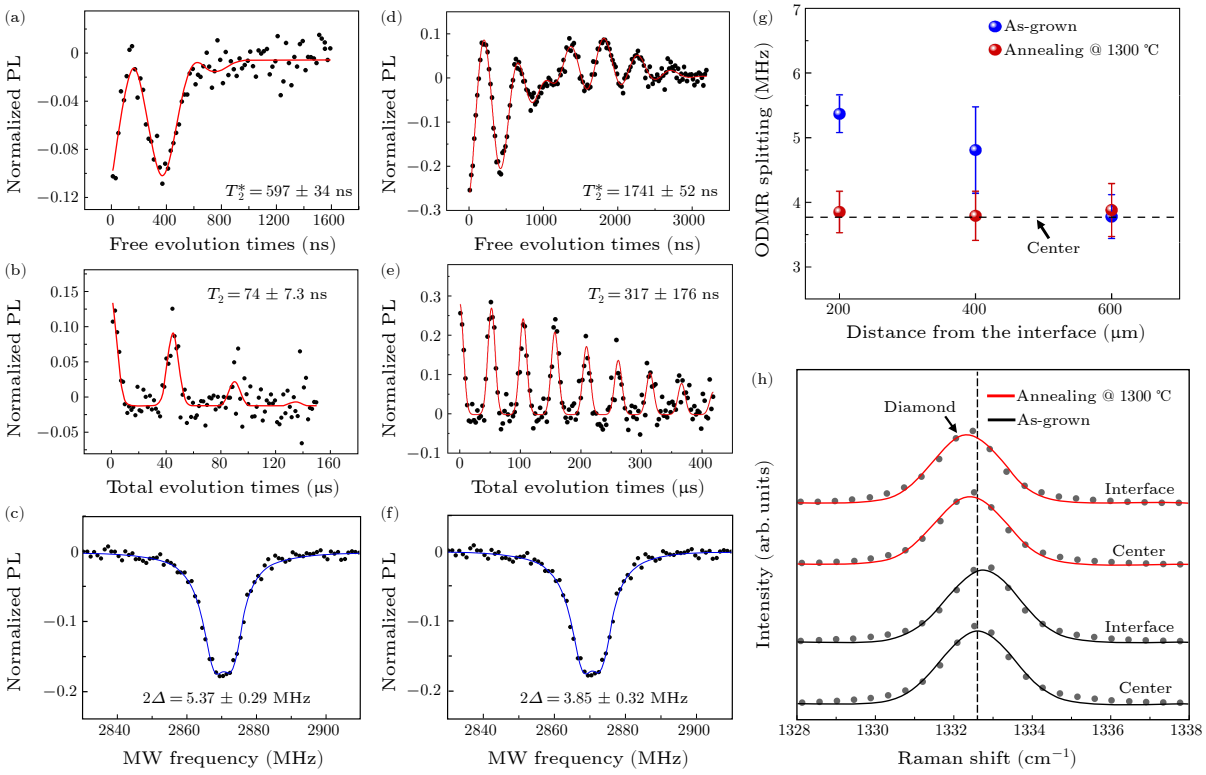

Fig. 3. Enhancement of spin coherence in NV$^-$ centers by HPHT annealing treatment. (a)–(c) Free-induction decay, spin echo signals and zero-field ODMR spectrum from a single NV$^-$ center located approximately 200 µm away from the interface in sample S1. (d)–(f) Free-induction decay, spin echo signals and zero-field ODMR spectrum of a single NV$^-$ center in 200 µm distant from the interface in sample S1 after annealing at 1300 ℃. Zero-field ODMR spectra in (c) and (f) were measured in the presence of Earth's magnetic field. The solid lines in (a)–(f) represent exponential fitting curves corresponding to the measured experimental data (black closed circles). Spin echo signal fitted by $y_1 e^{[-(t/T_2)^n]} + y_0$, where n is a free parameter, y_0, y_1 and T_2 and are fitting parameters. [23] The Ramsey signal was fitted by $e^{[-(t/T_2^*)^n]} \sum_{i=1}^{3} \cos(2f_i t)$, where n is a free parameter, f_i values correspond to level shifts from the host ^{14}N nuclear spin. [37] (g) Zero-field splitting of ODMR spectra from single NV$^-$ centers at varying distances from the interface. (h) Raman spectra obtained from interface and center of ⟨111⟩-growth sector before and after annealing at 1300 ℃.

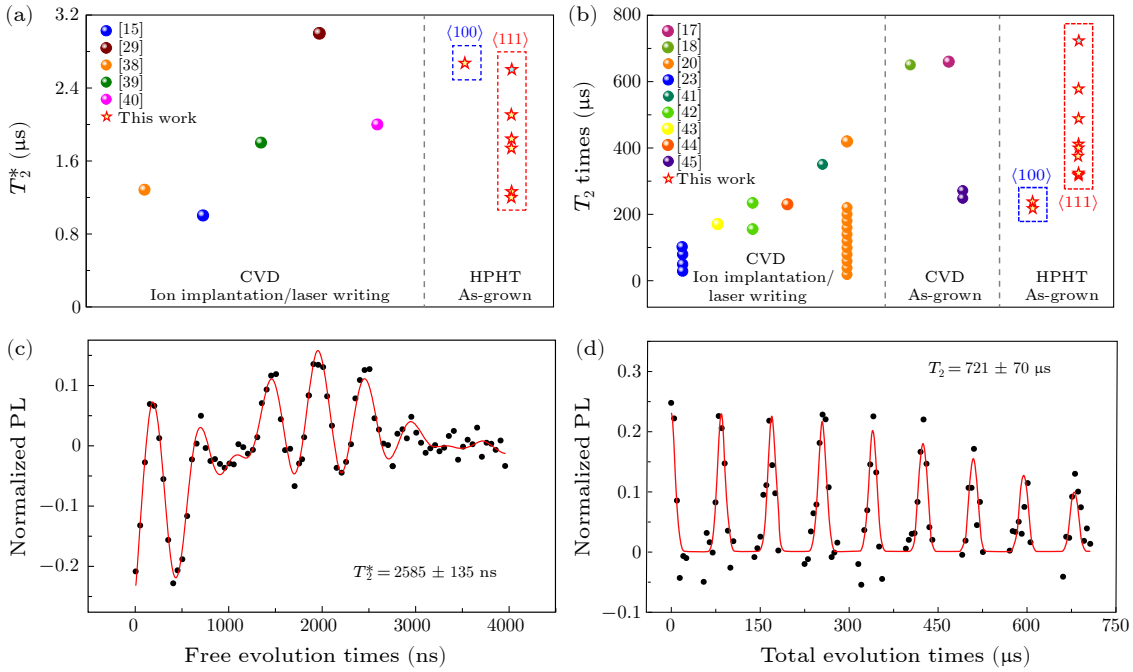

Fig. 4. Spin coherence of single NV$^-$ centers in HPHT diamonds. (a), (b) Comparison of the T_2^* and T_2 times for selected single NV$^-$ centers in HPHT diamonds with those reported in the literature for CVD samples. Yellow-filled stars denote single NV$^-$ centers created after high-pressure/high-temperature (HPHT) annealing, while blue-filled stars represent those naturally formed at the center of the ⟨111⟩-growth sector. (c), (d) FID, and spin echo signals of a single NV$^-$ center with T_2^* and T_2 times of 2.5 μs and 721 μs, respectively. The beating signal depicted in panel (c) arises from a strongly coupled ^{13}C nucleus. In contrast, the collapses and revivals illustrated in panel (d) are induced by the precession of the natural abundance ^{13}C nuclear spin bath within the applied hyperfine and dipolar magnetic fields.

including the central area of the ⟨111⟩-growth sector and across the entire ⟨100⟩-growth sector. We identified that the substantial stress field at the interface significantly contributes to the degradation of single NV$^-$ center spin coherence. By employing HPHT annealing, we effectively reduced this distortion of the lattice field, thereby enhancing coherence properties. Moreover, surrounding electric fields generated by adjacent defects, amplified by lattice stress, may also contribute to the degradation of coherence properties in single NV$^-$ centers.[46,47] Future research should prioritize accurate measurements conducted in environments shielded from the Earth's magnetic field to better understand these effects and develop strategies to enhance NV$^-$ spin coherence for quantum applications. Post-treatment, single NV$^-$ centers in the ⟨111⟩-growth sector consistently demonstrated long T_2 times exceeding 300 μs, with a maximum of 578 μs, while those in the ⟨100⟩-growth sector showed T_2 values above 200 μs. This highlights HPHT annealing as an effective method for generating high-coherence single NV$^-$ centers, with the ⟨111⟩-growth sector proving more favorable. Given that CVD diamond growth predominantly occurs along the ⟨100⟩ orientation, utilizing ⟨111⟩-oriented seed crystals to promote ⟨111⟩ growth may enhance coherence time. Additionally, we identified a naturally formed single NV$^-$ center in the as-grown ⟨111⟩-growth sector with an exceptional spin coherence time of 721 μs, one of the highest T_2 values recorded in diamonds with natural ^{13}C abundance.

These findings indicate that further reducing growth-induced external field is essential for enhancing the spin coherence of single NV$^-$ centers. Previous studies have shown that NV$^-$ centers in ^{13}C isotope-purified diamonds exhibit remarkable coherence properties, with T_2 times reaching 2.5 ms and T_2^* times reaching 1.4 ms.[48,49] Thus, employing HPHT treatment alongside other stress engineering techniques presents significant potential for advancing coherence properties. This work elucidates the formation mechanism of high-coherence single NV$^-$ centers in type-IIa HPHT diamonds, establishes a scalable fabrication method, and identifies key factors that govern the enhancement of NV$^-$ spin coherence. These insights offer valuable guidance for further improving NV$^-$ center coherence.

Acknowledgements. This work was supported by the National Natural Science Foundation of China (Grant Nos. 112374012 and 11974208) and Shandong Provincial Natural Science Foundation (Grant Nos. ZR2023JQ001 and tsqn202211128).

References

[1] Doherty M W, Manson N B, Delaney P, Jelezko F, Wrachtrup J, and Hollenberg L C L 2013 *Phys. Rep.* **528** 1

[2] Jelezko F and Wrachtrup J 2006 *Phys. Status Solidi A* **203** 3207

[3] Atatüre M, Englund D, Vamivakas N, Lee S Y, and Wrachtrup J 2018 *Nat. Rev. Mater.* **3** 38

[4] Awschalom D D, Hanson R, Wrachtrup J, and Zhou B B 2018 *Nat. Photon.* **12** 516

[5] Zu C, Wang W B, He L, Zhang W G, Dai C Y, Wang F, and Duan L M 2014 *Nature* **514** 72

[6] Ruf M, Wan N H, Choi H, Englund D, and Hanson R 2021 *J. Appl. Phys.* **130** 070901

[7] Liu G Q and Pan X Y 2018 *Chin. Phys. B* **27** 020304

[8] Pompili M, Hermans S L N, Baier S, Beukers H K C, Humphreys P C, Schouten R N, Vermeulen R F L, Tiggelman M J, dos Santos Martins L, Dirkse B, Wehner S, and Hanson R 2021 *Science* **372** 259

[9] Bradley C E, de Bone S W, Möller P F W, Baier S, Degen M J, Loenen S J H, Bartling H P, Markham M, Twitchen D J, Hanson R, Elkouss D, and Taminiau T H 2022 *npj Quantum Inf.* **8** 122

[10] Maze J R, Stanwix P L, Hodges J S, Hong S, Taylor J M, Cappellaro P, Jiang L, Dutt M V G, Togan E, Zibrov A S, Yacoby A, Walsworth R L, and Lukin M D 2008 *Nature* **455** 644

[11] Palm M L, Ding C, Huxter W S, Taniguchi T, Watanabe K, and Degen C L 2024 *Science* **384** 465

[12] Shi F, Zhang Q, Wang P, Sun H, Wang J, Rong X, Chen M, Ju C, Reinhard F, Chen H, Wrachtrup J, Wang J, and Du J 2015 *Science* **347** 1135

[13] Robledo L, Childress L, Bernien H, Hensen B, Alkemade P F A, and Hanson R 2011 *Nature* **477** 574

[14] Bernien H, Hensen B, Pfaff W, Koolstra G, Blok M S, Robledo L, Taminiau T H, Markham M, Twitchen D J, Childress L, and Hanson R 2013 *Nature* **497** 86

[15] Barry J F, Schloss J M, Bauch E, Turner M J, Hart C A, Pham L M, and Walsworth R L 2020 *Rev. Mod. Phys.* **92** 015004

[16] Dai J H, Shang Y X, Yu Y H, Xu Y, Yu H, Hong F, Yu X H, Pan X Y, and Liu G Q 2022 *Chin. Phys. Lett.* **39** 117601

[17] Mizuochi N, Neumann P, Rempp F, Beck J, Jacques V, Siyushev P, Nakamura K, Twitchen D J, Watanabe H, Yamasaki S, Jelezko F, and Wrachtrup J 2009 *Phys. Rev. B* **80** 041201

[18] Wong K C, Ng S L, Ho K O, Shen Y, Wu J, Lai K T, Leung M Y, Leung W K, Dasari D B R, Denisenko A, Wrachtrup J, and Yang S 2022 *Phys. Rev. Appl.* **18** 024044

[19] van Dam S B, Walsh M, Degen M J, Bersin E, Mouradian S L, Galiullin A, Ruf M, Ijspeert M, Taminiau T H, Hanson R, and Englund D R 2019 *Phys. Rev. B* **99** 161203

[20] Haruyama M, Onoda S, Higuchi T, Kada W, Chiba A, Hirano Y, Teraji T, Igarashi R, Kawai S, Kawarada H, Ishii Y, Fukuda R, Tanii T, Isoya J, Ohshima T, and Hanaizumi O 2019 *Nat. Commun.* **10** 2664

[21] Cui J M, Chen X D, Fan L L, Gong Z J, Zou C W, Sun F W, Han Z F, and Guo G C 2012 *Chin. Phys. Lett.* **29** 036103

[22] Wang X J, Fang H H, Sun F W, and Sun H B 2022 *Laser Photon. Rev.* **16** 2100029

[23] Chen Y C, Salter P S, Knauer S, Weng L, Frangeskou A C, Stephen C J, Ishmael S N, Dolan P R, Johnson S, Green B L, Morley G W, Newton M E, Rarity J G, Booth M J, and Smith J M 2017 *Nat. Photon.* **11** 77

[24] McLellan C A, Myers B A, Kraemer S, Ohno K, Awschalom D D, and Bleszynski Jayich A C 2016 *Nano Lett.* **16** 2450

[25] Orwa J O, Greentree A D, Aharonovich I, Alves A D C, Van Donkelaar J, Stacey A, and Prawer S 2010 *J. Lumin.* **130** 1646

[26] Mainwood A 1999 *Diamond Relat. Mater.* **8** 1560

[27] Chu Y, de Leon N P, Shields B J, Hausmann B, Evans R, Togan E, Burek M J, Markham M, Stacey A, Zibrov A S, Yacoby A, Twitchen D J, Loncar M, Park H, Maletinsky P, and Lukin M D 2014 *Nano Lett.* **14** 1982

[28] Acosta V M, Bauch E, Ledbetter M P, Santori C, Fu K M C, Barclay P E, Beausoleil R G, Linget H, Roch J F, Treussart F, Chemerisov S, Gawlik W, and Budker D 2009 *Phys. Rev. B* **80** 115202

[29] Rondin L, Tetienne J P, Hingant T, Roch J F, Maletinsky P, and Jacques V 2014 *Rep. Prog. Phys.* **77** 056503

[30] Smith J M, Meynell S A, Bleszynski Jayich A C, and Meijer J 2019 *Nanophotonics* **8** 1889

[31] Zhang X, Liu K Y, Li F, Liu X, Duan S, Wang J N, Liu G Q, Pan X Y, Chen X, Zhang P, Ma Y, and Chen C 2023 *Adv. Funct. Mater.* **33** 2309586

[32] Huang G F, Jia X P, Ma H A, Bai H B, Yin J W, and Hu Y G 2012 *Chin. Phys. Lett.* **29** 106102

[33] Zaitsev A M, Kazuchits N M, Kazuchits V N, Moe K S, Rusetsky M S, Korolik O V, Kitajima K, Butler J E, and Wang W 2020 *Diamond Relat. Mater.* **105** 107794

[34] Zang C Y, Huang G F, Ma H A, and Jia X P 2007 *Chin. Phys. Lett.* **24** 2991

[35] Zhang X, Song J, Xing X, Zhang C, Sun Y, and Liu X 2024 *Int. J. Refract. Met. Hard Mater.* **119** 106509

[36] Ashfold M N R, Goss J P, Green B L, May P W, Newton M E, and Peaker C V 2020 *Chem. Rev.* **120** 5745

[37] Childress L, Gurudev Dutt M V, Taylor J M, Zibrov A S, Jelezko F, Wrachtrup J, Hemmer P R, and Lukin M D 2006 *Science* **314** 281

[38] Blinder R, Mindarava Y, Tran T H, Momenzadeh A, Yang S, Siyushev P, Sumiya H, Tamasaku K, Osaka T, Morishita N, Takizawa H, Onoda S, Hara H, Jelezko F, Wrachtrup J, and Isoya J 2024 *Commun. Mater.* **5** 224

[39] Chen X Y, Qiu C D, Lu Y N, Liu G Q, Ruan D, Zhang F, and Long G 2023 *Phys. Rev. B* **108** 174111

[40] Hong S, Grinolds M S, Pham L M, Le Sage D, Luan L, Walsworth R L, and Yacoby A 2013 *MRS Bulletin* **38** 155

[41] Gaebel T, Domhan M, Popa I, Wittmann C, Neumann P, Jelezko F, Rabeau J R, Stavrias N, Greentree A D, Prawer S, Meijer J, Twamley J, Hemmer P R, and Wrachtrup J 2006 *Nat. Phys.* **2** 408

[42] Wang J, Zhang W, Zhang J, You J, Li Y, Guo G, Feng F, Song X, Lou L, Zhu W, and Wang G 2016 *Nanoscale* **8** 5780

[43] Chen Y C, Griffiths B, Weng L, Nicley S S, Ishmael S N, Lekhai Y, Johnson S, Stephen C J, Green B L, Morley G W, Newton M E, Booth M J, Salter P S, and Smith J M 2019 *Optica* **6** 662

[44] Li L, Schröder T, Chen E H, Walsh M, Bayn I, Goldstein J, Gaathon O, Trusheim M E, Lu M, Mower J, Cotlet M, Markham M L, Twitchen D J, and Englund D 2015 *Nat. Commun.* **6** 6173

[45] Balasubramanian P, Osterkamp C, Brinza O, Rollo M, Robert-Philip I, Goldner P, Jacques V, Jelezko F, Achard J, and Tallaire A 2022 *Carbon* **194** 282

[46] Yu Y H, Zhang R Z, Xu Y, Chen X Q, Zheng H, Li Q, Liu R B, Pan X Y, Budker D, and Liu G Q 2024 *Phys. Rev. Appl.* **21** 044051

[47] Mittiga T, Hsieh S, Zu C, Kobrin B, Machado F, Bhattacharyya P, Rui N Z, Jarmola A, Choi S, Budker D, and Yao N Y 2018 *Phys. Rev. Lett.* **121** 246402

[48] Herbschleb E D, Kato H, Maruyama Y, Danjo T, Makino T, Yamasaki S, Ohki I, Hayashi K, Morishita H, Fujiwara M, and Mizuochi N 2019 *Nat. Commun.* **10** 3766

[49] Balasubramanian G, Neumann P, Twitchen D, Markham M, Kolesov R, Mizuochi N, Isoya J, Achard J, Beck J, Tissler J, Jacques V, Hemmer P R, Jelezko F, and Wrachtrup J 2009 *Nat. Mater.* **8** 383